VSP

Composite Interfaces 16 (2009) 201–218

COMPOSITE INTERFACES
www.brill.nl/ci

Thermal Degradation Behavior, Permeation Properties and Impact Response of Polyethylene/Organo-montmorillonite/(Ethylene Methacrylic Acid) Ternary Nanocomposites

Valeria Pettarin [a,*], Laura Fasce [a], Victor Rodriguez Pita [b], Marcos Lopes Dias [b] and Patricia Frontini [a]

[a] Instituro de Investigaciones en Ciencia y Tecnología de Materiales INTEMA, Universidad Nacional de Mar del Plata, Juan B. Justo 4302, B7608FDQ Mar del Plata, Argentina
[b] Instituto de Macromoléculas Professora Eloisa Mano IMA, Universidade Federal do Rio de Janeiro, Caías Postal 68525, 21945-970 Rio de Janeiro, Brasil

Received 22 August 2007; accepted 3 September 2008

Abstract
Through this work we explored the effect of melt compounding a commercial grade of HDPE with organoclays of different precedence using EMAA as compatibilizing agent on the thermal behavior, barrier properties and biaxial impact response of composites. Morphology was examined by XRD and TEM. Crystalline structure was examined by DSC. Thermal behavior was evaluated by TGA. Barrier properties to low-molecular-weight penetrants were experimentally determined employing a gravimetric technique. Mechanical properties under impact conditions were evaluated by instrumented puncture tests. Intercalated nanocomposites were obtained. Throughout the thermal degradation of the nanocomposites in oxidant atmosphere a charring process of the PE, which is normally a non-char-forming polymer, was observed. The addition of OMMT improves barrier properties due to its contribution to tortuosity path and to the reduction of molecular mobility. Impact properties were only slightly reduced by nanocomposite formation. Results demonstrate that EMAA did not improve exfoliation, but it enhanced polymer–organoclay interactions giving rise to better thermal and permeation properties, without detriment of impact response.

Keywords
PE, ionomer, nanocomposite, thermal degradation, permeation, impact response

1. Introduction

The promise of hybrid composites engineered from polymers and nanoscale components (such as carbon nanotubes, nanoclays and nanofibers) presents a challenge to researchers in applied materials science. In recent years, polymer–clay nanocom-

* To whom correspondence should be addressed. E-mail: pettarin@fi.mdp.edu.ar

 DOI:10.1163/156855409X402885

posites have attracted much academic and industrial interest because of the anticipated improvements in properties, such as stiffness, gas barrier, flammability, thermal resistance among others [1, 2] due to the interaction between polymer and clay at the nanoscale level [3]. Nanocomposites may be prepared either by polymerization of a monomer in the presence of clay or by blending a polymer with clay. In either case, the sodium cation which occupies the gallery space in the clay must be ion-exchanged with an 'onium' salt which contains at least one long organic chain to render the gallery space sufficiently organophilic to permit the entry of the polymer into this gallery space. However, it has been claimed that only the presence of clay is not enough to improve properties [4]. The properties of all heterogeneous materials are determined by the same four factors: characteristics of components, composition, structure and interfacial interactions [5]. Therefore it is also necessary to create an intimate interaction between the polymer and the clay platelets to improve properties.

Polyethylene (PE) is one of the most widely used polyolefin polymers, which possesses a fortuitous combination of many useful properties: light weight, low cost, high-chemical resistance, low dielectric constant and losses, good processability, etc. Interest in polyolefin nanocomposites has emerged in an attempt to improve PE performance in engineering applications. The main problem to overcome in the production of clay–polyolefin nanocomposites is that polymers like PE lack suitable interactions with the aluminosilicate surface of the clay, even if clays are organically modified [6–8]. Therefore, addition of an appropriate compatibilizer [4] or chemical modification of the polymer matrix [9] is also required. Another novel and attractive proposal recently reported in literature to improve clay polymer interaction is to copolymerize the olefin monomer with polar monomers like methacrylic acid or acrylic acid [10–13]. It has been claimed that the random incorporation of as little as 1 mol% of ionic functionalities along the polymer backbone could enhance interactions between the matrix polymer and the organoclay. The use of a commercially available thermoplastic like ethylene methacrylic acid copolymer (EMAA) in order to improve matrix clay interactions appears appealing and promising: EMAA contains both ethylene segments — that have a specific interaction with polyethylene — and methacrylic acid segments — that may have specific interactions with organoclays — and so it may heighten interactions between PE and organoclays.

Dispersions of nanoscale reinforcements in polymers are already entering the marketplace in automotive applications. For instance, since 2002 General Motors and Honda have used polyolefin/nanoclay composites in exterior and interior parts of their GMC Safari, Chevrolet Astro van, GM Hummer H2 SUT and Honda Acura TL. Among the many auto exterior, interior and under-hood applications for which nanocomposites appeared suited are fascias, rocker covers, side trims, grilles, hood louvers, instrument panels, seat/IP foams, door inners, pillar covers, vertical and horizontal body and closure panels, engine shrouds, fan shrouds, air intakes, fuel tanks and fuel lines. If nanocomposites are intended to be used as fuel tanks or

liners, the overall barrier performance to low-molecular-weight penetrants including gasoline, flammability and impact properties are of crucial importance and they should meet the stringent application criteria.

In this work, we explored the effect of melt compounding a commercial grade of HDPE with organoclays of different precedence using EMAA as compatibilizing agent on the thermal behavior, barrier properties and biaxial impact response.

2. Experimental

2.1. Materials and Sample Preparation

The composite matrix was a blow grade high density PE (40055L, by PBB Polisur). Three Na^+-MMT with differences in exchange capability (Wyoming Bentonite B-3378 by Sigma (SW), Brazilian clay from Campina Grande, Paraiba (B) and Argentinean montmorillonite (A); see Table 1) were modified with hexadecyl trimethyl ammonium chloride (HDTMA) CTAC-50-CT, by GENAMIN, and dried in an oven for 16 h at 60°C in order to obtain organically modified montmorillonites (OMMT), denoted here as OSW, OB and OA, respectively. A commercial ethylene/methacrylic acid copolymer (Nucrel® 1202HC, $T_m = 99$°C, acid groups = 12%, MFI = 1.5 g/10 min (2.16 kg/190°C) provided by DuPont was selected as modifier, denoted here as EMAA. Composites were prepared by melt blending in a twin screw counter-rotating extruder Rheocord 9000-Haake, at 60 rpm and a temperature profile of 190-195-205-210°C. Used composition was 3 wt% of OMMT and 0 or 1 wt% of EMAA [14]. Pellets of each material were compression-molded into 3 mm thick plaques at 190°C.

2.2. Morphology and Crystalline Structure

Morphologies of the obtained composites were studied by combined techniques: X-ray diffraction (XRD) and transmission electronic microscopy (TEM). Crystalline structure was assessed by differential scanning calorimetry (DSC).

XRD was carried out using a Philips X'PERT MPD diffractometer (Cu K_α radiation $\lambda = 1.5418$ Å, 40 kV, 40 mA). The interlayer distance of clay was calculated from the (001) peak by using the Bragg equation.

Table 1.
Characteristics of montmorillonites

MMT	Water content (%)	Ion exchange capacity (meq/100 g clay)	Specific area BET (m^2/g)	Accompanying minerals (Q = quartz, K = kaolin)	Particle size after organophilization (μm)
SW	11.4	124	40	Q	7.4
B	11.7	151	82	Q, K	7.4
A	11.7	110	70	Q, K	7.4

Micrographs were obtained from a TEM Jeol 100 CX microscope using an acceleration voltage of 200 kV. Samples were ultramicrotomed at room temperature with a diamond knife to a 70 nm thick section.

DSC were performed in a Perkin Elmer Pyris 1 device using 10 mg nominal sample weight, at a scanning rate of 10°C/min from 50°C to 200°C under nitrogen atmosphere. The crystalline fraction of PE in the composites was calculated as:

$$x_c = \frac{\Delta H}{(1-\phi)\Delta H^0}, \tag{1}$$

where ΔH is the apparent enthalpy of fusion per gram of composite, ΔH^0 is the heat of fusion of a 100% crystalline PE taken as 293 J/g [15], and ϕ is the weight fraction of the filler (clay and EMAA) in the composites.

2.3. Thermal Degradation

Thermogravimetric analysis (TGA) was carried out in a Shimadzu Electrobalance. Experiments were conducted at a constant rate of 10°C/min from room temperature to 650°C both in nitrogen and air flow. About 2 mg of materials were loaded into the container. From TGA curves we have extracted the pertinent information, which includes the onset temperature of the degradation, usually taken as the temperature at which 10% degradation occurs, $T_{0.1}$, the midpoint temperature of the degradation, another measure of thermal stability, $T_{0.5}$, and the fraction of non-volatile that remains at 600°C, denoted as char. From DTG curves, the maximum decomposition temperature (T_{max}) is obtained. TGA results were also used to study the condensed phase reaction during combustion processes, since it has been demonstrated that the chemical evolution moving from the bulk of the specimen to the burning zone is the same as the one revealed in TGA experiments at increasing temperatures [16].

2.4. Gasoline Uptake

Relative gasoline uptake was experimentally determined employing a gravimetric technique. Specimens from each material were weighed in the dry stage and immersed in a gasoline simulate (50/50 wt% toluene/*n*-hexane solution) at room temperature. Each sample was frequently taken out of the solution and weighed. The relative gasoline uptake (M_t) was taken as:

$$M_t = \frac{W_w - W_d}{W_d}, \tag{2}$$

where W_w is the specimen weight after an exposure time, t, and W_d is the weight in the dry stage, respectively.

The diffusion coefficient (D) was calculated for the initial stages of sorption assuming application of Fick's law for a single-phase diffusion process *via*:

$$\frac{M_t}{M_m} = \frac{4}{\sqrt{\pi}}\sqrt{\frac{Dt}{h^2}}, \tag{3}$$

where h is the specimen thickness and M_m is the saturation or equilibrium gasoline content. The sorption coefficient (S) was taken from the equilibrium plateau of the sorption curves, and the related permeability coefficient (P) was calculated using the relation

$$P = DS. \tag{4}$$

2.5. Biaxial Impact Response

Disk specimens of 80 mm in diameter for impact measurements were machined from plaques. Impact testing was performed using a Fractovis Ceast falling weight machine according to ASTM D 3763-02. A high-speed dart weighing 18.49 kg was employed. All tests were performed using a probe with hemispherical end of 5 mm diameter equipped with a force-sensing load cell with a full range of 9100 N. The disk specimens were held in place with an annular ring. Tests were conducted at room temperature and at an impact velocity of 3 m/s.

The thickness related perforation energy of evaluated materials was obtained from the absorbed energy during impact event U, given by the numerical integration of load–displacement curves as U/B, where B is the thickness of the disc. Disc maximum strength σ_d is evaluated as:

$$\sigma_d = 2.5\frac{P_{max}}{B^2}, \tag{5}$$

with P_{max} the maximum load attained in the test, and the disc modulus E_d as:

$$E_d = 0.145(1-\nu^2)\left(\frac{\Delta P}{\Delta x}\right)\frac{D^2}{B^3}, \tag{6}$$

where ν is Poisson's coefficient, $\Delta P/\Delta x$ is the initial slope of the load–displacement curve and D the disc diameter.

In order to characterize the plastic yielding and elastic deformation under impact conditions of the obtained composites we used the ductile ratio parameter, DR, proposed by Fowler and Baker [17] and modified by Liu and Baker [18]:

$$DR = \frac{(U_t - U_m)}{U_t}, \tag{7}$$

where $(U_t - U_m)$ is the energy of plastic deformation after yield, U_m is the absorbed energy up to the maximum force, and U_t the total absorbed energy.

3. Results and Discussion

3.1. Morphology and Crystalline Structure

The d-spacing values between layers of clays, organoclays and composites obtained from XRD traces are shown in Table 2. After treatment with HDTMA, the d-spacing of organoclays increased by approximately 8 Å (70%), maintaining the original difference among them. For some composites (PE/OB and

Table 2.
d-spacing of clay layers obtained from XRD analysis, and thermal properties obtained from DSC results

Material	*d*-spacing (Å)	T_m (°C)	x_c
PE	–	136	0.65
SW	11.9	–	–
OSW	19.2	–	–
PE/OSW	20.1	137	0.62
PE/OSW/EMAA	14.3	133	0.64
B	13.1	–	–
OB	21.6	–	–
PE/OB	–	140	0.62
PE/OB/EMAA	–	136	0.64
A	12.6	–	–
OA	20.1	–	–
PE/OA	20.7	144	0.61
PE/OA/EMAA	15.8	141	0.63

PE/OB/EMAA), no characteristic basal diffraction peak of the organoclay appears in the range of $2\theta = 2$–$10°$, while for others (PE/OSW, PE/OA, PE/OA/EMAA and PE/OSW/EMAA) a weak and broad peak can be observed in XRD patterns with a maximum at low 2θ angle (around 4°). Results obtained from XRD measurements are never sufficient to define the exfoliation degree of nanocomposites, because of the possibility of disordering of the clay. Thus, characterization by TEM is also required. TEM micrographs reveal that, in all composites, clay platelets are mostly intercalated (see the example shown in Fig. 1(a)): even some tough exfoliated platelets can be found (as shown in Fig. 1(b)), i.e., intercalation and partial exfoliation may occur during processing. We believe that the lack or weakness of an X-ray peak is the result of a more random orientation of clay particles rather than the indication of a more exfoliated morphology; TEM analysis supports this hypothesis.

When EMAA was added, the interlayer distance diminished, indicating some degree of interaction between OMMT and EMAA. Competitive interactions can take place during mixing: PE or EMAA may enter into the galleries of the filler or surfactant diffuses out of clay dissolving in matrix or in EMAA. The organic modifier of the clay (HDTMA) is ionically bonded to the surface and cannot diffuse out of the interspace without debonding. This latter case implies a reaction with an acid, like EMAA. The result would be a protonated (even if only partially) clay with a collapse of the interlayer space, a fact that was observed in XRD. We therefore think that mostly this occurs in the case of PE/OMMT/EMAA composites, i.e., the acidic carboxyl groups ($–COO^-H^+$) of EMAA interact with the ammonium cations inside the clay galleries removing part of them from the galleries [19].

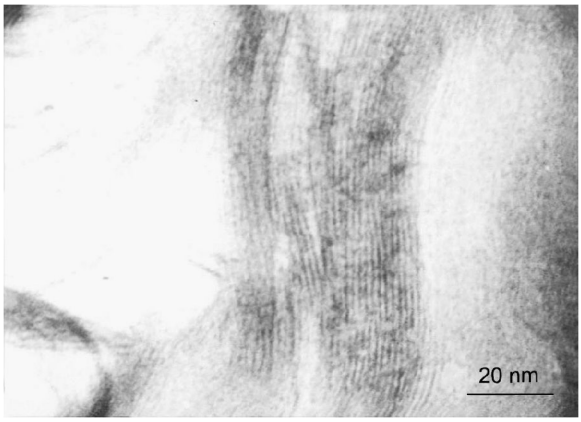

(a)

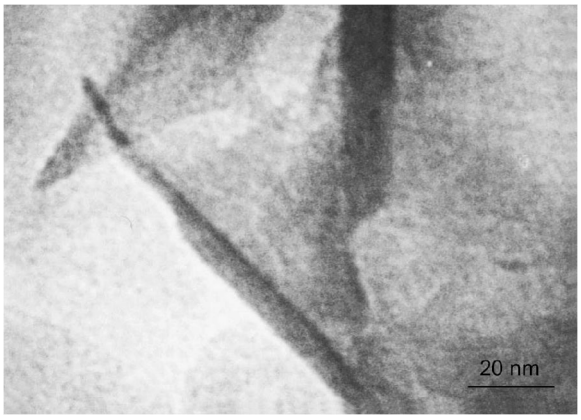

(b)

Figure 1. TEM pictures of PE/OSW/EMAA.

Thermal properties deduced from DSC traces are reported in Table 2. The addition of OMMT slightly diminishes the crystalline degree, x_c, and increases the melting temperature (T_m), demonstrating that the solid clay particles have little influence on the crystallization behavior. The melting peak of PE–OMMT composites is slightly wider than the pure PE peak indicating a broader distribution of crystal sizes. This phenomenon has been attributed to the crystal size changes, probably due to the barrier effect of the dispersed layers that limit the crystallization of the PE [20]. It is found that when EMAA is added to composites, x_c, T_m and peak shape are drawn near to the initial state, i.e., pure PE without OMMT and EMAA, as if clay particles were not present.

3.2. Thermal Degradation Behavior

TGA and DTGA curves under nitrogen atmosphere for composites and the polymer matrix (pure PE and PE/EMAA) are shown in Fig. 2. In Fig. 3 the same results are shown under air atmosphere. TGA and DTGA data are displayed in Table 3.

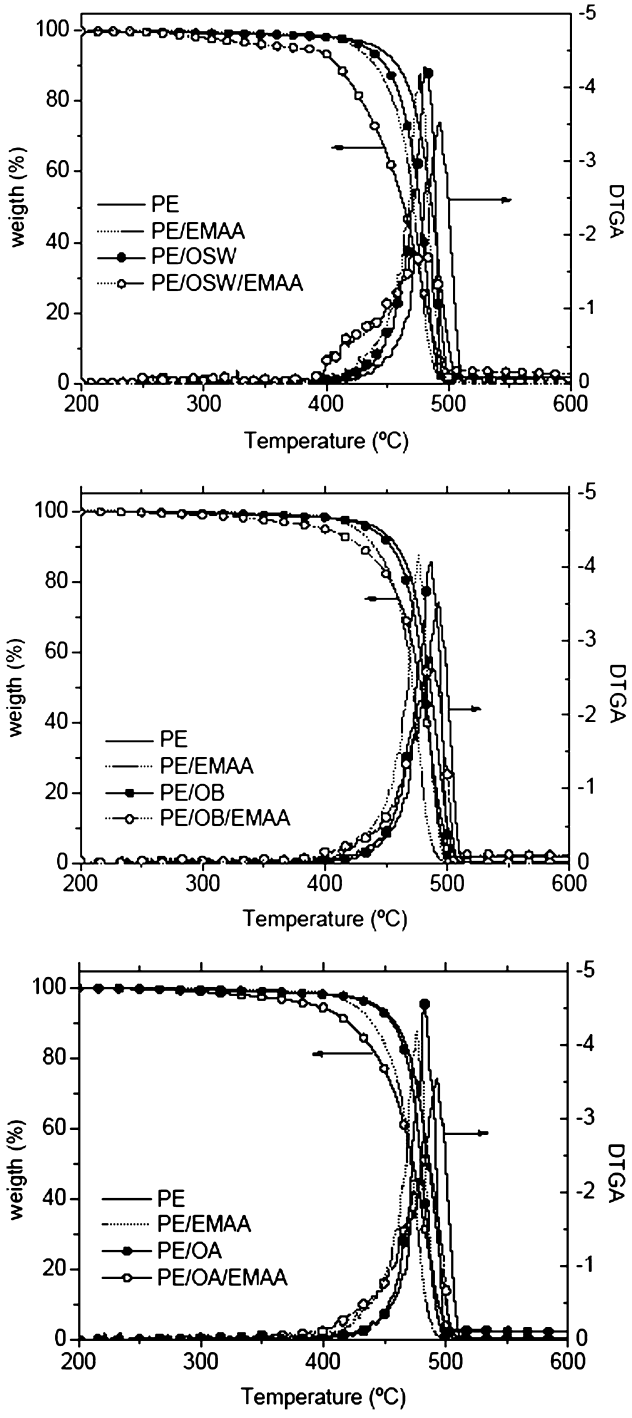

Figure 2. TGA and DTGA curves of PE and composites under nitrogen atmosphere.

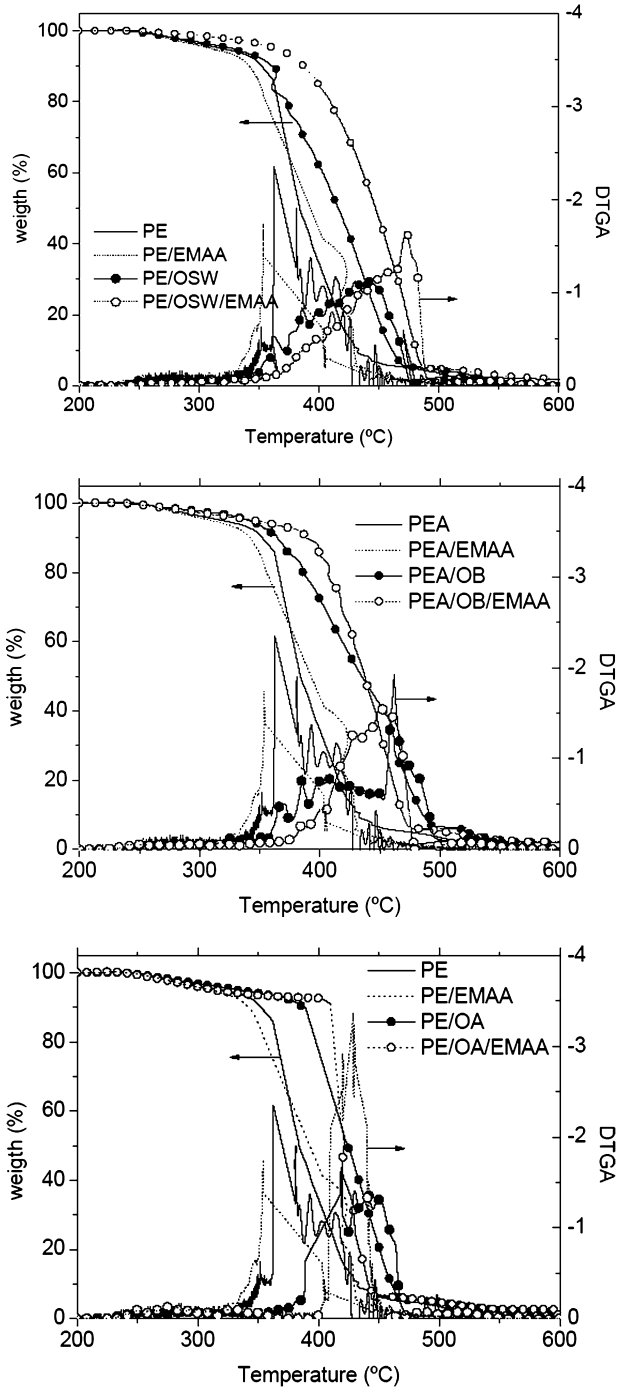

Figure 3. TGA and DTGA curves of PE and composites under oxidative atmosphere.

Table 3.
TGA and DTGA data for PE and its nanocomposites

Material	$T_{0.1}$ (°C)	$T_{0.5}$ (°C)	T_{max} (°C)	Char (%)
Under nitrogen atmosphere				
PE	458.9	486.4	492.7	0.2
PE/EMAA	440.3	471.8	476.6	0.2
PE/OSW	448.8	476.8	480.8	1.9
PE/OSW/EMAA	409.8	463.9	477.9	2.5
PE/OB	454.2	481.5	486.7	1.8
PE/OB/EMAA	429.1	478.4	486.4	2.4
PE/OA	456.8	480.3	488.7	2.3
PE/OA/EMAA	421.4	473.5	483.8	2.3
Under air				
PE	352.4	383.9	362.5	0.4
PE/EMAA	342.2	394.1	353.9	0.3
PE/OSW	361.1	416.3	449.3	1.9
PE/OSW/EMAA	387.5	447.1	474.3	2.1
PE/OB	364.8	435.1	450.9	2.0
PE/OB/EMAA	389.3	437.7	462.1	2.2
PE/OA	388.1	424.2	419.2	2.2
PE/OA/EMAA	409.3	421.2	428.8	2.7

Consistently with related literature, OMMT addition has almost no effect on the thermal degradation of PE under nitrogen atmosphere [4, 21, 22]. However, EMAA does provoke changes in initial stages of degradation of PE, i.e., $T_{0.1}$, of composites. Moreover, when OMMT and EMAA are compounded with PE, there is a perceptible reduction in resistance to thermal degradation. However, the maximum in the rate of weight loss remains similar. PE leaves no residue at temperature higher than 500°C while PE/OMMT and PE/OMMT/EMAA leave the same amount of residue corresponding to the inorganic part of the organoclay added. It seems that EMAA catalyzes the degradation of polymer matrix, and that there is a synergist effect when EMAA is combined with OMMT in PE, reducing the thermal stability of polymer/clay nanocomposites under non-oxidative conditions.

On the other hand, strong positive effects on thermal degradation were observed under oxidative atmosphere. Above 350°C, PE is subjected, in air, to a strong weight loss to form about 6 wt% residue at 450°C, which is completely oxidized to volatile products. PE decomposition temperatures increase with the addition of OMMT: $T_{0.1}$ increases about 13°C for OB and OSW, and near 40°C for OA. Subsequent addition of EMAA increased $T_{0.1}$ another 25°C for all clays. The organoclay presence shields the polymer degradation from the action of oxygen, increasing the thermal stability in oxidative conditions. EMAA increases further this protection. The improvement in thermal degradation by OA was higher than by OSW and OB,

with PE/OA/EMAA composite the one showing the best thermal degradation performance.

The thermal stability difference observed in air could be attributed to two different effects: the OMMT mass transport barrier and the suppression of the molecular mobility. Regarding the barrier effect, it is been stated that when matrix–clay interaction is good, a barrier action can improve the thermal stability of polymer/clay composites [23]. The barrier effect increases during the volatilization of degradation products and forms chars on the reticular layers of the silicate [4, 24], which involves two key phenomena [16]:

(a) The barrier effect due to diffusion of both the volatile thermo-oxidation products from the polymer to the gas phase and oxygen from the gas phase to the polymer. This barrier effect increases during volatilization owing to ablative reassembly of the reticular layers of the silicate on the surface of the polymer. Thus oxidative dehydrogenation leads to conjugate double bond sequences that transform the polymer in a conjugated polyene that evolves on heating to thermally stable charred structures [25].

(b) The shield formed on the surface of the nanocomposites protects the polymer underneath from oxygen, preserving the long chain structure at elevated temperatures.

The other positive effect is the reduction in the molecular motion: it was stated that MMT layers enhance the thermal stability of polymers through suppression of molecular mobility [26]. Studies carried out over several polymers indicated that the long chain molecular motion in the nanocomposites encounters a markedly larger energy barrier than pristine polymers [27–30]. That is, at the same temperature, the nanocomposite would have lower molecular mobility than the virgin polymer. In other words, translational motion in the polymer–clay system requires a larger degree of cooperativity. The extra cooperativity in polymer–clay nanocomposites is induced by the clay sheets that anchor several polymer chains, making their individual motion mutually dependent. Because the molecular mobility is the major factor that contributes to the transport of reactive species within the polymer, the nanocomposites are likely to have lower reactivity and, therefore, greater chemical and thermal stability than virgin polymer. Moreover, it was also stated that the intercalated nanostructure in polymer/layered silicate nanocomposites, like the one exhibited by our nanocomposites, was crucial to enhance the thermal stability [28].

On the other hand, the alkylammonium cations in the organoclay could suffer decomposition following the Hofmann elimination reaction [31, 32], and its product would catalyze the degradation of polymer matrixes [33]. In addition, the clay itself can also catalyze the degradation of polymer matrixes [34, 35]. These two actions would reduce the thermal stability of polymer/clay nanocomposites.

In summary, the organoclay has opposing functions in the thermal stability of the polymer/clay nanocomposites: on the one side the barrier effect and the restriction of molecular mobility improve the nanocomposite thermal stability, and on the other side the catalytic effect towards the degradation of the polymer matrix decreases the

thermal stability of the nanocomposite. If the first effects are dominant, an improvement in thermal stability is obtained [36]. It has been claimed that the sole presence of clay is not enough to promote these effects [4]. The intimate interaction between the polymer and the clay platelets is also necessary.

EMAA increases the thermal-oxidation stability of the PE/OMMT composites. Our results suggest that EMAA increases the efficiency of char formation and reduction of molecular mobility, i.e., EMAA improves polymer/organoclay interactions. This effect is particularly relevant in polymers such as PE, which is a non-char-forming polymer with large molecular mobility.

Keeping in mind the validity of TGA to study the condensed phase reactions of combustion process, and that during the combustion the polymer matrix is subjected to a temperature gradient as the flame front is left over, it also can be predicted that the protective char/clay layer would be formed in PE/OMMT/EMAA composites before the flame invests it directly. After that, the flame would have to propagate through this layer suffering a slow down.

3.3. Gasoline Uptake

M_t as a function of the immersion time $\sqrt{t}$ is shown in Fig. 4 for all composites while all coefficient values are shown in Table 4. Examination of S, D and P values shows that there is a noticeable improvement in the resistance to gasoline permeation by addition of OMMT. The gasoline permeation resistance of all nanocomposites is better than those of the pure PE, while the lowest sorption and permeability coefficient was obtained for PE/OA/EMAA.

It has been claimed that the decrease in the permeability coefficient depends on polymer structure, crystalline fraction, crystallites size, clay content and its dispersion [37], and that the polymer–clay interface and interactions are the dominant factors that contribute to improve the polymer barrier properties [38, 39]. In our case, the crystalline fraction, and polymer structure is essentially the same in pure PE and composites, not affecting the permeability properties. However, upon addition of OMMT, the barrier properties improve. This is due to its contribution to the tortuosity path. These results are in concordance with previous works in which it was reported that intercalated composites exhibited a noticeable drop in permeability coefficient, since the perturbation area for a layered silicate extends far more widely than the chain dimensions [40]. Regarding PE/OMMT/EMAA improvement in barrier properties with respect to PE/OMMT composites, it seems that the addition of EMAA gives place to a better interphase between PE and OMMT, assembling a structure which hinders molecules diffusion.

3.4. Impact Response

Typical force–displacement traces obtained under impact conditions are shown in Fig. 5, and U/B, σ_d, E_d and DR are reported in Table 5.

As expected, binary composites slightly reduce the thickness related perforation energy. When EMAA is added to composites, a slight increase in U/B is observed.

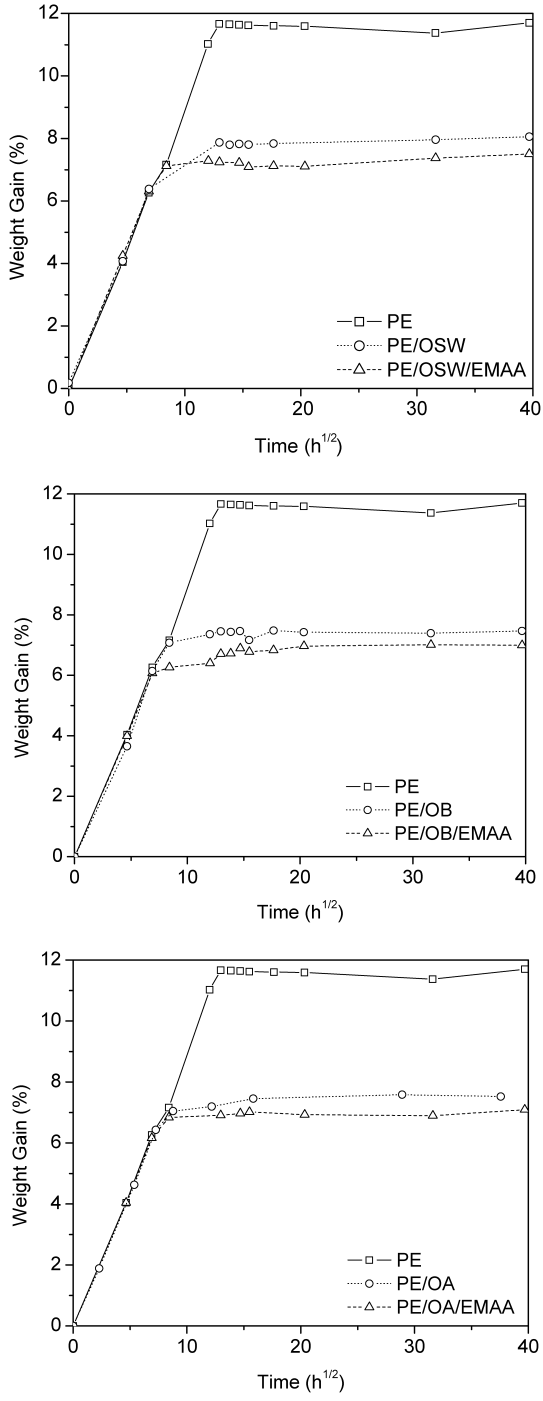

Figure 4. Relative weight gain for all nanocomposites exposed to gasoline simulant.

Table 4.
Sorption (S), diffusion (D) and permeability (P) coefficients of materials to gasoline

Material	S (g/g)	$D \times 10^{12}$ (m^2/s)	$P \times 10^{13}$ (m^2/s)
PE	0.116	4.82	5.59
PE/OSW	0.0795	4.53	3.60
PE/OSW/EMAA	0.0737	3.87	2.85
PE/OB	0.0746	4.19	3.13
PE/OB/EMAA	0.0697	4.46	3.11
PE/OA	0.0758	4.21	3.19
PE/OA/EMAA	0.0689	4.06	2.80

The ductile ratio is the relative percentage of energy absorbed in plastic deformation out of the total impact energy. It is an indication of the 'ductility' of the polymer. For an ideal brittle material which does not exhibit any plasticity, the U_t is equal to U_m and the DR is equal to zero. For an ideal ductile material which exhibits little elasticity, the $U_t \gg U_m$ and DR approaches one. The values of DR of general viscoelastic materials are between zero and one. Composites exhibit lower DR with the addition of OMMT. However, with the subsequent addition of EMAA, DR increases again, recovering the values of PE matrix. σ_d and E_d of all PE/OMMT composites are larger than the ones of PE, due to the reinforcement effect of clay. Regarding PE/OMMT/EMAA composites, they exhibit larger σ_d and E_d than PE/OMMT composites, indicating that the interaction between OMMT and PE is enhanced by EMAA.

Again, mechanical properties are highly dependant on interface properties, and it seems that EMAA improves the interaction between clay and PE, and consequently improves mechanical properties under impact conditions in comparison with that ones of PE/OMMT composites.

4. Conclusions

During the processing of PE nanocomposites, interactions take place among all components, including the compounds used for the organophilization of the clay. Complete exfoliation definitely does not take place under the conditions used in this study, but some intercalation or limited delamination cannot be excluded completely.

Throughout the thermal degradation of the nanocomposites in oxidant atmosphere an improvement in resistance to thermal degradation was observed, which was attributed to a charring process of the PE, which is normally a non-char-forming polymer, and a reduction of PE molecular mobility. The presence of the clay promotes this improvement. In PE/OMMT/EMAA composites, where an intimate contact between the polymer chains and the clay platelets is achieved, the necessary reactions take place efficiently leading to the formation of an amount

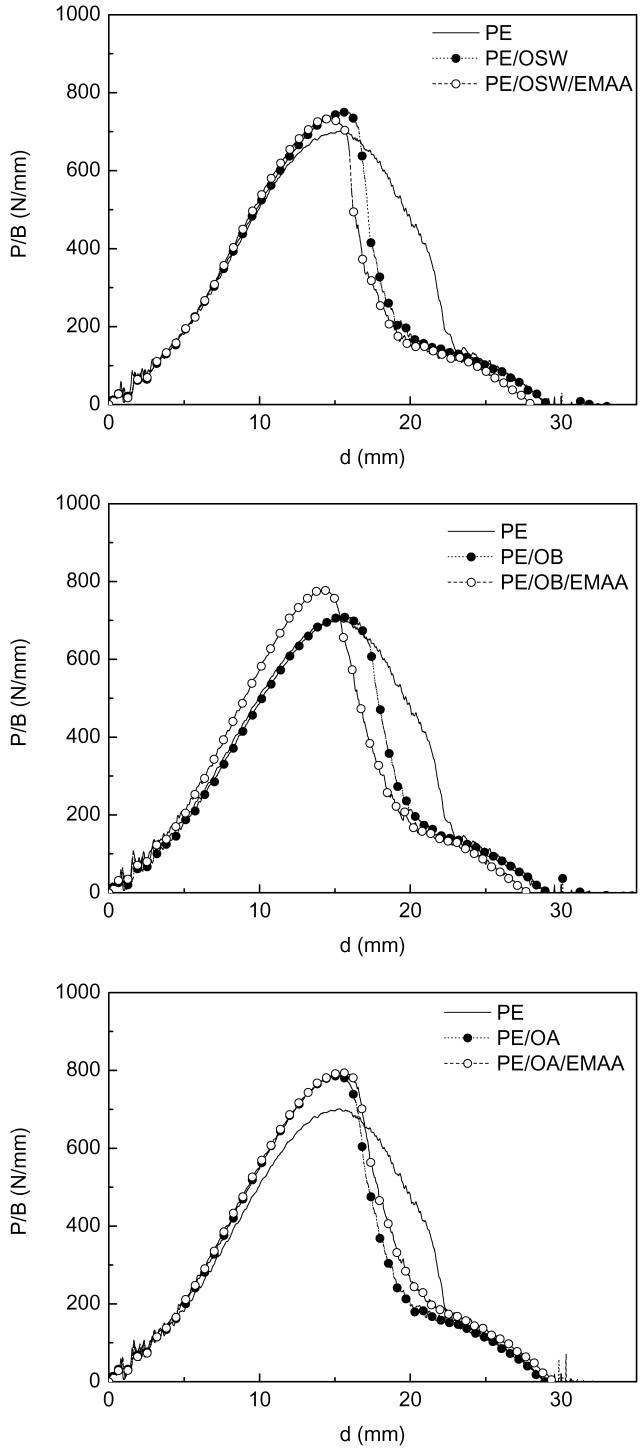

Figure 5. Thickness related force *vs*. displacement traces obtained in biaxial impact tests.

Table 5.
Mechanical properties under biaxial impact conditions

Material	U/B (J/mm)	σ_d (MPa)	E_d (GPa)	DR
PE	10.05	627	7.55	0.44
PE/OSW	8.07	677	9.01	0.38
PE/OSW/EMAA	9.23	789	11.92	0.45
PE/OB	8.55	730	10.28	0.36
PE/OB/EMAA	9.51	735	12.52	0.47
PE/OA	9.32	849	12.51	0.37
PE/OA/EMAA	9.55	895	13.44	0.37

of char large enough to link the clay platelets which leads to the formation of a continuous material. Also, clay sheets anchor several polymer chains more efficiently, making their individual motion mutually dependent. Therefore, the thermal behavior of ternary nanocomposites is improved.

The addition of OMMT improves the barrier properties due to its contribution to tortuosity path. Furthermore, in the PE/OMMT/EMAA composites, the sorption and permeability coefficient were reduced, due to the better interphase between PE and OMMT, which results in a more closed structure that prevents molecules from diffusing through.

Impact strength and modulus of PE is enhanced by nanocomposite formation, while thickness related energy to break and DR are only slightly reduced by OMMT addition, recovering PE values when EMAA is added.

In summary, although EMAA does not improve exfoliation, it enhances polymer–organoclay interactions giving rise to better thermal and permeation properties, without detriment of impact response.

Based on the obtained results we conclude that nanocomposites prepared from PE and OMMT compatibilized with EMAA may be particularly suitable for automotive applications.

Acknowledgements

The authors would like to thank CONICET and ANPCyT from Argentina for financial support, and also SECyT/CAPES bilateral collaboration research program for financial supporting research missions.

References

1. P. Bala, B. K. Samantaray and S. K. Srivastava, Synthesis and characterization of Na-montmorillonite-alkylammonium intercalation compounds, *Mater. Res. Bull.* **35**, 1717–1724 (2000).

2. T. G. Gopakumar, J. A. Lee, M. Kontopoulou and J. S. Parent, Influence of clay exfoliation on the physical properties of montmorillonite/polyethylene composites, *Polymer* **43**, 5483–5491 (2002).
3. P. C. LeBaron, Z. Wang and T. J. Pinnavaia, Polymer-layered silicate nanocomposites: an overview, *Appl. Clay Sci.* **15**, 11–29 (1999).
4. M. Zanetti and L. Costa, Preparation and combustion behavior of polymer/layered silicate nanocomposites based upon PE and EVA, *Polymer* **45**, 4367–4373 (2004).
5. B. Pukánszky, Review: interfaces and interphases in multicomponent materials: past, present and future, *Eur. Polym. J.* **41**, 645–662 (2005).
6. H. G. Jeon, H. T. Jung, S. W. Lee and S. D. Hudson, Morphology of polymer/silicate nanocomposites, *Polym. Bull.* **41**, 107–113 (1998).
7. N. Furuichi, Y. Kurokawa, K. Fujita, A. Oya, H. Yasuda and M. Kiso, Preparation and properties of polypropylene reinforced by smectite, *J. Mater. Sci.* **31**, 4307–4310 (1996).
8. J. Heinemann, P. Reichert, R. Thomann and R. Mulhaupt, Polyolefin nanocomposites formed by melt compounding and transition metal catalyzed ethene homo- and copolymerization in the presence of layered silicates, *Macromol. Rapid Commun.* **20**, 423–430 (1999).
9. K. H. Wang, M. H. Choi, C. M. Koo, Y. S. Choi and I. J. Chung, Synthesis and characterization of maleated polyethylene/clay nanocomposites, *Polymer* **42**, 9819–9826 (2001).
10. G. D. Barber, B. H. Calhoun and R. B. Moore, Poly(ethylene terephthalate) ionomer based clay nanocomposites produced *via* melt extrusion, *Polymer* **46**, 6706–6714 (2005).
11. P. R. Start and K. A. Mauritz, Surlyn®/silicate nanocomposite materials *via* a polymer *in situ* sol–gel process: morphology, *J. Polym. Sci. Part B: Polym. Phys.* **41**, 1563–1571 (2003).
12. R. K. Shah, D. L. Hunter and D. R. Paul, Nanocomposites from poly(ethylene-co-methacrylic acid) ionomers: effect of surfactant structure on morphology and properties, *Polymer* **46**, 2646–2662 (2005).
13. J. A. Lee, M. Kontopoulou and S. Parent, Synthesis and characterization of polyethylene-based ionomer nanocomposites, *Polymer* **46**, 5040–5049 (2005).
14. V. Pettarin, P. M. Frontini, V. J. R. R. Pita, M. L. Dias and F. Valenzuela Diaz, Polyethylene/(organo-montmorillonite) composites modified with ethylene/methacrylic acid copolymer: morphology and mechanical properties, *Compos. Part A: App. Sci. and Manuf.* **39**, 1822–1828 (2008).
15. B. Wunderlich, *Macromolecular Physics*, Vol. 3. Academic Press, New York, USA (1980).
16. M. Zanetti, P. Bracco and L. Costa, Thermal degradation behavior of PE/clay nanocomposites, *Polym. Degrad. Stabil.* **85**, 657–665 (2004).
17. M. Fowler and W. E. Baker, Rubber toughening of polystyrene through reactive blending, *Polym. Engng Sci.* **28**, 1427–1433 (1988).
18. T. M. Liu and W. E. Baker, Instrumented dart impact evaluation of linear low density polyethylene at controlled impact energy, *Polym. Engng Sci.* **31**, 753–763 (1991).
19. K. Bagdi, P. Müller and B. Pukánszky, Thermoplastic starch/layered silicate composites: structure, interaction, properties, *Composite Interfaces* **13**, 1–17 (2006).
20. M. Alexandre and P. Dubois, Polymer-layered silicate nanocomposites: preparation, properties and uses of a new class of materials, *Mater. Sci. Engng* **28**, 1–63 (2000).
21. J. Zhang and C. Wilkie, Preparation and flammability properties of polyethylene–clay nanocomposites, *Polym. Degrad. Stabil.* **80**, 163–169 (2003).
22. J. Zhang, D. Jiang and C. Wilkie, Polyethylene and polypropylene nanocomposites based upon an oligomerically clay, *Thermochimica Acta* **430**, 107–113 (2005).
23. L. Qiu, W. Chen and B. Qu, Morphology and thermal stabilization mechanism of LLDPE/MMT and LLDPE/LDH nanocomposites, *Polymer* **47**, 922–930 (2006).

24. C. M. L. Preston, G. Amarasinghe, J. L. Hopewell, R. A. Shanks and Z. Mathys, Evaluation of polar ethylene copolymers as fire retardant nanocomposite matrices, *Polym. Degrad. Stabil.* **84**, 533–544 (2004).
25. W. H. Starnes, *Developments in Polymer Degradation*. Applied Science Publishers, Barking, UK (1981).
26. A. Leszczynska, J. Njuguna, K. Pielichowski and J. R. Banerjee, Polymer/montmorillonite nanocomposites with improved thermal properties: Part I. Factors influencing thermal stability and mechanisms of thermal stability improvement, *Thermochimica Acta* **453**, 75–96 (2007).
27. D. Lee, S. H. Lee, K. Char and J. Kim, Expansion distribution of basal spacing of the silicate layers in polyaniline/Na^+-montmorillonite nanocomposites monitored with X-ray diffraction, *Macromol. Rapid Commun.* **21** 1136–1139 (2000).
28. D. Lee and K. Char, Thermal degradation behavior of polyaniline in polyaniline/Na^+-montmorillonite nanocomposites, *Polym. Degrad. Stabil*. **75**, 555–560 (2002).
29. K. Chen, M. A. Susner and S. Vyazovkin, Effect of the brush structure on the degradation mechanism of polystyrene–clay nanocomposites, *Macromol. Rapid Commun.* **26**, 690–695 (2005).
30. S. Vyazovkin and I. Dranca, A DSC study of, and relaxations in, a PS-Clay System, *J. Phys. Chem. B* **108**, 11981–11987 (2004).
31. M. Zanetti, G. Camino, R. Thomann and R. Mülhaupt, Synthesis and thermal behavior of layered silicate–EVA nanocomposites, *Polymer* **42**, 4501–4507 (2001).
32. W. Xie, Z. Gao, W. P. Pan, D. Hunter, A. Singh and R. Vaia, Thermal degradation chemistry of alkyl quaternary ammonium montmorillonite, *Chem. Mater.* **13**, 2979–2990 (2001).
33. H. Qin, Z. Zhang, M. Feng, F. Gong, S. Zhang and M. Yang, The influence of interlayer cations on the photo-oxidative degradation of polyethylene/montmorillonite composites, *J. Polym. Sci. Part B: Polym. Phys.* **42**, 3006–3012 (2004).
34. H. Qin, S. Zhang, C. Zhao, M. Feng, M. Yang and Z. Shu, Thermal stability and flammability of polypropylene/montmorillonite composites, *Polym. Degrad. Stabil.* **85**, 807–813 (2004).
35. M. Zanetti, B. Pierangiola and C. Luigi, Thermal degradation of PE/clay nanocomposites, *Polym. Degrad. Stabil.* **85**, 657–665 (2004).
36. C. Zhao, H. Qin, F. Gong, M. Feng, S. Zhang and M. Yang, Mechanical, thermal and flammability properties of polyethylene/clay nanocomposites, *Polym. Degrad. Stabil.* **87**, 183–189 (2005).
37. L. K. Sahu, N. A. D'Souza and B. Gnade, Permeability of polymer nanocomposites, in: *Proc. ANTEC 2006*, American Chemical Society (Ed.), Charlotte, North Carolina, USA, pp. 1554–1558 (2006).
38. T. J. Pinnavaia and G. W. Beall, *Polymer–Clay Nanocomposites*. Wiley, Chichester, UK (2001).
39. A. Sorrentino, M. Tortora and V. Vittoria, Diffusion behavior in polymer–clay nanocomposites, *J. Polym. Sci. Part B: Polym. Phys.* **44**, 265–274 (2006).
40. A. Ranade, N. D'Souza, B. Gnade and J. A. Ratto, Permeability measurement of polymers and layered silicate nanocomposites, in: *Proc. ANTEC 2004*, Chicago, USA, pp. 2405–2409 (2004).